ACS OMEGA

http://pubs.acs.org/journal/acsodf

Article

Characteristics and Sintering Mechanisms of Iron Ores with a High Proportion of High-Al_2O_3 Limonite

Zhikai Liang, Jun Chen,* Zhucheng Huang,* and Boyang Huang

Cite This: *ACS Omega* 2023, 8, 15951−15959

Read Online

ACCESS | Metrics & More | Article Recommendations

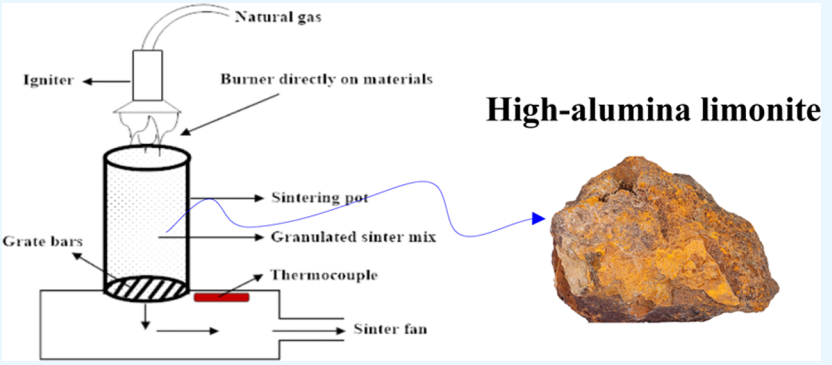

ABSTRACT: In this study, a sintering test of high-alumina limonite from Indonesia, matched with an appropriate magnetite concentration, is performed. The sintering yield and quality index are effectively improved by optimizing the ore matching and regulating the basicity. For the optimal coke dosage of 5.8% and basicity of 1.8, the tumbling index of the ore blend is found to be 61.5% and the productivity is 1.2 t/(h·m^2). The main liquid phase in the sinter is the silico-ferrite of calcium and aluminum (SFCA), followed by a mutual solution, both of which maintain the sintering strength. However, when the basicity is increased from 1.8 to 2.0, the production of SFCA is found to increase gradually, whereas the mutual solution content decreases dramatically. A metallurgical performance test of the optimal sinter sample demonstrates that the sinter can meet the requirements of small- and medium-sized blast furnace smelting, even for high-alumina limonite ratios of 60.0−65.0%, thereby greatly reducing the sintering production costs. The results of this study are expected to provide theoretical guidance for the practical high-proportion sintering of high-alumina limonite.

INTRODUCTION

Due to the depletion of low-impurity iron ore deposits, along with the increase in demand for iron ore in China, the iron and steel enterprises in that country have imported an increasing amount of foreign iron ore in recent years.[1,2] Iron ores from Australia, South Africa, and India account for a large proportion of these imports and usually exhibit high -alumina contents.[3,4] Furthermore, there is no effective mineral processing technique for removing alumina from high-alumina iron ores.[5,6]

Meanwhile, an iron ore sinter is a crucial material for the iron-making process, and its chemical, physical, and metallurgical properties significantly impact the blast furnace (BF) performance.[9] In turn, the main materials used for a sinter are iron ore fines, and their chemical compositions play a critical role in the sintering process. Due to the low reactivity of alumina-bearing minerals and the high viscosity of the primary melts, the presence of alumina in the sinter mix requires much heat for its assimilation, thereby delaying the sintering process.[10−12] Hence, it is essential to understand the role of alumina and its effects on the sintering process and sinter quality. Moreover, the development of an efficient application for high-alumina iron ores could provide a new way to reduce production costs.[7,8] In this respect, when the maximum Al_2O_3 content in the system is 1.5%, an alumina-to-silica ratio of <1.0 is considered to be ideal for BF operation.[13,14] For a sinter with a high alumina content, the addition of a substantial amount of flux is recommended in order to obtain more low-melting bonding phases and fluid slag in the BF process.[15−17] Therefore, increased basicity (CaO/SiO_2) is necessary for high-Al_2O_3 systems.[18]

The major bonding phase in high-Al_2O_3 systems is a complex calcium ferrite known as the silico-ferrite of calcium and aluminum (SFCA). This is essentially iron oxide with a

Received: November 30, 2022
Accepted: April 11, 2023
Published: April 27, 2023

Table 1. Chemical Analysis of Raw Materials (wt %)

	TFe	Fe_2O_3	FeO	CaO	SiO_2	Al_2O_3	MgO	S	LOI
H	50.2	71.3	0.4	1.0	3.1	9.6	0.2	0.1	14.3
J	48.0	67.8	0.7	1.6	3.2	11.2	0.9	0.1	14.5
K	58.3	83.1	0.2	0.7	4.3	3.1	0.2	0.03	8.4
D	64.2	63.7	25.2	0.9	6.5	1.4	0.4	0.08	1.8
T	66.5	65.4	26.6	1.0	1.7	2.8	1.7	0.02	0.7
dolomite	1.0	1.4	0.0	29.0	1.5	0.2	20.9	0.0	47.0
limestone	0.4	0.6	0.0	51.8	2.7	0.8	0.9	0.0	43.2

Table 2. Industrial Analysis and Ash Analysis of Coke Breeze (wt %)[a]

proximate analysis					ash analysis				
name	FC_{ad}	V_{ad}	A_{ad}	S	TFe	SiO_2	Al_2O_3	CaO	MgO
content	85.2	2.5	11.6	0.7	11.4	41.1	27.6	5.8	1.8

[a]FC_{ad}: fixed carbon; V_{ad}: volatile matter; A_{ad}: ash.

Table 3. Particle Size Composition of Raw Materials (wt %)[a]

	+5 mm	−5 + 3 mm	−3 + 1 mm	−1 + 0.5 mm	−0.5 + 0.1 mm	−0.1 mm
H	6.6	7.5	34.5	11.4	23.7	16.3
J	2.3	6.9	34.8	18.9	22.6	14.5
K	7.4	3.8	44.4	20.0	14.0	10.4
D	0.0	0.0	0.0	0.0	2.1	97.9
T	0.0	0.0	0.0	0.8	7.6	91.6
dolomite	2.6	10.2	49.9	7.4	9.6	20.3
limestone	3.2	10.5	55.4	9.1	12.3	9.6
coke breeze	5.2	2.8	32.8	25.5	12.5	21.2

[a]The dolomite, limestone, and coke powder contained, respectively, 97.4, 96.8, and 94.8% of particles of <5 mm.

minimum of 3% Al_2O_3 and plays an important role in influencing key sinter quality parameters such as the tumbler index (TI), reducibility, and reduction degradation index (RDI).[19,20] The SFCA can be divided on the basis of composition and morphology into two main types: (i) a high-Fe, low-Si form $SiO_{2(low)}$-$Fe_2O_{3(high)}$-CaO-Al_2O_3 designated SFCA-I and (ii) a low-Fe, high-Si form $SiO_{2(high)}$-$Fe_2O_{3(low)}$-CaO-Al_2O_3 designated SFCA.[21,22] A study by T. Umadevi indicated that an increase in the alumina content (2.0−5.5%) in sinter hematite resulted in an increase in both the SFCA and pore phase content, whereas the magnetite and silicate phase contents were decreased.[18] In addition, both the sinter productivity and tumbler index (TI) were found to decrease, while the reducibility increased with the increase in alumina content. Meanwhile, M.M. Hessien reported that a small increase in the alumina content of the sinter blend can have substantial adverse effects on the strength and reduction degradation characteristics of the final sinter.[23,24]

In brief, due to the low reactivity of Al_2O_3 in high-alumina systems, along with the high viscosity of the liquid phase,[25,26] a lot of heat is inevitably consumed during the sintering process, thereby increasing the fuel consumption,[27,28] delaying the process,[29,30] and degrading the metallurgical properties of the sinter (i.e., lowering the strength, increasing the RDI, and degrading the droplet properties).[18,31] Meanwhile, limonite is one of the principal types of iron ore and has a low melting point. Consequently, if the fuel ratio is increased, the liquid phase is more abundantly generated, and both the permeability of the sintered high-temperature zone and the quality index of the sinter are reduced.[9,32,33] Therefore, the sintering of high-alumina limonite is characterized by a low sintering speed, low productivity, loose organization of the sinter cake, low yield, and high fuel consumption.

Moreover, the Al_2O_3 content has a very important impact on the formation and crystallization of the SFCA, and this effect involves many factors, including (but not limited to) the basicity and operating conditions. Hence, a strategy for increasing the limiting content of Al_2O_3 in order to promote the SFCA formation and inhibit its adverse effects on the sintering strength and low-temperature reduction degradation is worthy of study.

Consequently, this study is aimed at realizing the efficient utilization of high-alumina iron ore, using high-alumina limonite as the research object. The sintering optimization of high-alumina limonite is performed in order to evaluate the applicability of this kind of ore in a given blending scheme and under suitable sintering conditions.

EXPERIMENTAL SECTION

Materials. The physical and chemical properties of the raw materials used in the experiment are listed in Tables 1−3. The ferrous materials included three types of imported high-Al_2O_3 limonite fines from the Limonite Mining Company, Indonesia, in which the particles of <5 mm accounted for 93.4, 97.7, and 92.6% (designated H, J, and K, respectively), and two types of domestic magnetite concentrates obtained from the Baowu Iron and Steel Group, China, which had lower alumina contents and >83.0% particles with sizes <200 mesh (designated D and T, respectively). The dolomite ($xCaCO_3{\cdot}yMgCO_3$) and limestone ($CaCO_3$) fluxes, along with the coke breeze fuel, were obtained from the Baowu Iron and Steel Group, China.

Methods. As shown schematically in Figure 1, the sintering experiments were performed using a laboratory sinter pot with a diameter of 200 mm and a height of 700 mm and having a

https://doi.org/10.1021/acsomega.2c07659
ACS Omega 2023, 8, 15951−15959

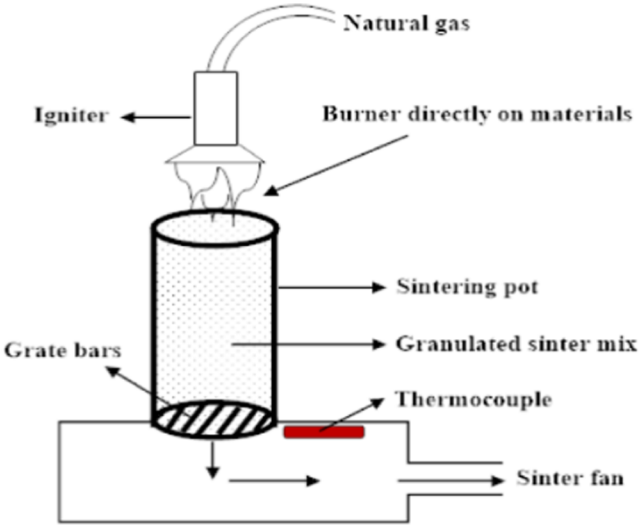

Figure 1. Schematic diagram of the sintering pot.

removable grate bar at the bottom. The sintering mix and the hearth layer charges were fixed at about 32.0 and 2.0 kg, respectively. The sintering test conditions are listed in Table 4, and the proportions of raw materials for the five ore batches are indicated in Table 5.

Table 4. Parameters of the Sintering Test

items	conditions
coke breeze (−3 mm)	>90%
dolomite and limestone (−3 mm)	>85%
basicity (CaO/SiO_2)	1.8−2.0
MgO	2.3%
coke breeze rate	5.5−6.1%
mix moisture	9.5−12.0%
granulation time	180 s
ignition suction	−5 kPa
ignition temperature	1050 ± 30 °C
ignition time	90 s
ignition heat preservation temperature	980 ± 20 °C
ignition heat preservation time	60 s
sintering suction	−8 kPa
sinter return proportioning	30%
cooling time	5 min

Table 5. Mix Proportion for Different Ore Batching Schemes

ore blending schemes	H	J	K	D	T
1	100.0	0.0	0.0	0.0	0.0
2	0.0	100.0	0.0	0.0	0.0
3	45.0	10.0	15.0	25.0	5.0
4	45.0	15.0	0.00	35.0	5.0
5	50.0	15.0	0.0	25.0	10.0

A flow chart of the sintering test is presented in Figure 2, and the operating parameters are listed in Table 6. For the sintering process, the mass batching method was adopted, in which the water for mixing was added manually three times, followed by mixing and granulating in a drum mixer (Φ600 mm × L1400 mm; 20 r/min). After granulation, the mixture was transferred to a sintering cup (Φ150 mm × H720 mm) with bedding material to give a total layer height of 700 mm. The gas used for the ignition was natural gas. The sintering time was defined as the time taken for the sintering waste gas to reach its maximum and just start to cool down. When the sintering endpoint was reached, the material was discharged after cooling for 5 min, then broken by a single-tooth roller crusher, and tested for shatter strength, particle size distribution, and tumbling strength. Additionally, a final sinter sample was taken for chemical analysis and determination of its metallurgical properties and mineralogical phases.

The formulae for calculating the evaluation indexes (vertical sintering speed, productivity, and tumbling strength) are as follows

$$V_{\perp} = H/t \tag{1}$$

$V_{\perp}$—vertical sintering speed, mm·min^{-1};
H—height of the sinter layer, mm;
t—sintering time, min.

$$r = 7.65 \times 10^4 M/(D^2 \cdot t) \tag{2}$$

r—productivity, t·m^{-2}·h^{-1};
M—weight of the final sinter, kg;
D—inner diameter of the sintering cup, mm.

$$P = (m_1 - 1)/(m_0 - 1) \times 100\% \tag{3}$$

P—yield, %;
m_1—weight of +5 mm size fraction, kg;
m_0—total weight of the sinter, kg.

$$\mathrm{TI} = M_1/M_0 \times 100\% \tag{4}$$

TI—tumbling strength, %;
M_1—weight of the sinter put into the drum, kg;
M_0—weight of +6.30 mm size fraction after trundling and screening, kg.

Characterization. The metallurgical performance was evaluated using the reducibility test, low-temperature reduction degradation index (RDI) test, and high-temperature soft melting properties test. The reducibility test was conducted in accordance with the international standard ISO 7215-2015: Iron ores for blast furnace feedstocks − Determination of the reducibility by the final degree of reduction index. The RDI test was conducted in accordance with ISO 4696-1-2015: Iron ores for blast furnace feedstocks − Determination of low-temperature reduction-disintegration indices by static method − Part 1: Reduction with CO, CO_2, H_2, and N_2. The high-temperature soft melting properties test was performed using a 30:70 mix of CO and N_2 as the reducing gas at a flow rate of 15 L/min and a load of 980 × 10^2 Pa. During the test, the samples were heated up to 900 °C at a rate of 10 °C/min, maintained at a constant temperature of 900 °C for 30 min, and then heated above 900 °C at a rate of 5 °C/min to determine the temperatures at which the total heights of the ore samples shrink by 10 and 40% (T_{ss} and T_{es}) and the temperature at which the liquid phase begins to drip (T_D). Additionally, the microstructural characteristics of the sinter were examined by using an environmental scanning electron microscope (ESEM) equipped with an EDAX energy-dispersive X-ray (EDX) spectrometer. The chemical composition of the sinter was determined by chemical dissolution analysis at the Changsha Research Institute of Mining and Metallurgy in Hunan Province, China.

RESULTS AND DISCUSSION

Characteristics of High-Alumina Limonite Sintering. In this test, the ore blending was performed at a set basicity of 1.9

https://doi.org/10.1021/acsomega.2c07659
ACS Omega 2023, 8, 15951−15959

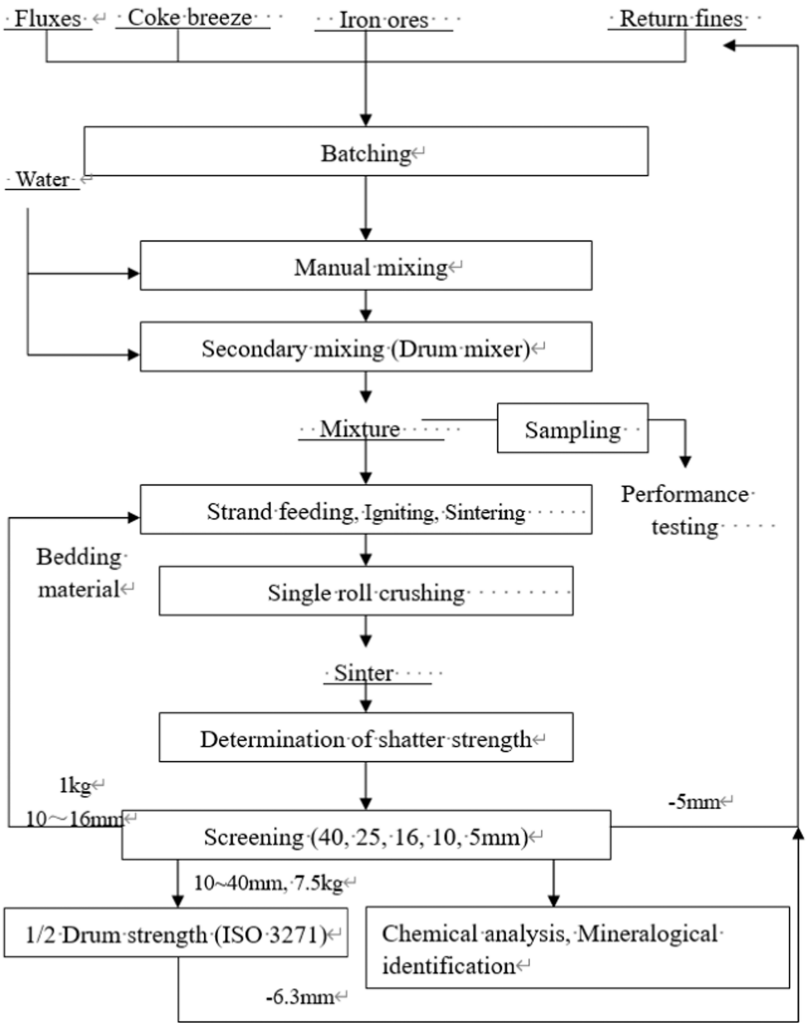

Figure 2. Flow chart of the sintering test.

Table 6. Operating Parameters of the Sintering Test

blending time/min		height of sinter layer/mm		sintering ignition		
I	II	total material height	bedding material	temperature /°C	time/min	negative pressure /kPa
manpower	3	700	~20	1050 ± 30	1.5	5
keep warm after ignition				sintering	cooling	
temperature/°C	time/min	negative pressure/kPa		negative pressure/kPa	time/min	
980 ± 20	1	8		8	5	

Table 7. Sintering Quality Indexes of High-Alumina Limonite

schemes	mix moisture/%	coke dosage/%	sintering speed/mm·min^{-1}	yield/%	tumbling strength/%	productivity/t·m^{-2}·h^{-1}
1	10.5	5.5	25.8	61.1	54.2	1.0
	11.0	5.5	28.3	61.2	54.6	1.1
	11.5	5.5	30.2	56.8	55.0	1.0
	11.0	5.8	30.9	63.2	53.1	1.2
	11.0	6.1	26.7	67.8	54.5	1.1
	11.0	6.4	27.8	66.3	52.1	1.1
2	12.0	6.1	25.2	55.1	49.6	0.8
	12.0	6.4	24.7	65.2	55.5	1.0
	12.0	6.7	23.1	71.1	58.3	1.0
	12.0	7.0	21.6	70.6	44.3	0.9
	11.0	6.7	19.7	68.0	51.2	0.4
	11.5	6.7	21.1	71.2	59.0	0.9

https://doi.org/10.1021/acsomega.2c07659
ACS Omega 2023, 8, 15951−15959

Table 8. Sintering Quality Index of High-Alumina Limonite Ore Blending

schemes	mix moisture/%	coke dosage/%	sintering speed/mm·min^{-1}	yield/%	tumbling strength/%	productivity/t·m^{-2}·h^{-1}
3	9.0	5.8	28.0	71.1	54.6	1.4
	9.0	6.1	30.6	73.4	55.2	1.6
	9.0	6.4	28.9	71.9	50.0	1.4
	8.0	6.1	20.9	75.5	51.8	1.1
	8.5	6.1	25.3	73.5	55.9	1.3
4	8.5	5.5	21.9	72.6	51.7	1.3
	8.5	5.8	21.7	74.1	56.6	1.2
	8.5	6.1	22.3	75.2	52.1	1.2
	8.0	5.8	15.6	57.0	42.0	0.7
	9.0	5.8	27.2	72.1	53.9	1.4
5	8.5	5.5	21.9	69.2	55.9	1.0
	8.5	5.8	22.0	73.3	59.1	1.2
	8.5	6.1	24.3	71.3	53.2	1.2
	8.0	5.8	20.3	71.9	56.8	0.9
	9.0	5.8	22.3	68.8	58.8	0.9

Table 9. Sintering Quality Index of Optimized Test

basicity	mix moisture/%	coke dosage/%	sintering speed/mm·min^{-1}	yield/%	tumbling strength/%	productivity/t·m^{-2}·h^{-1}
1.8	9.0	5.8	22.7	75.3	61.5	1.20
1.9	8.5	5.8	22.0	73.3	59.1	1.17
2.0	8.5	5.8	22.7	75.0	60.3	1.18

Table 10. Main Mineral Composition of Sinter/%

basicity	Fe_2O_3	Fe_3O_4	SFCA	SS	Olivine	magnesium ferrite	calcium silicate	CaO	vitreous
1.8	21.0	37.3	19.4	14.5	1.3	1.6	2.2	0.6	2.2
1.9	23.3	36.3	23.1	6.6	1.4	2.1	2.3	2.8	2.2
2.0	23.9	33.2	25.1	5.7	1.3	2.3	2.4	3.8	2.4

and an MgO content of 2.3%. The effects of varying the moisture content and coke dosage of the high-alumina H and J limonite fines on the specific quality indexes of the sinters are listed in Table 7.

Here, the sintering process of high-alumina limonite powder in the absence of magnetite powder is seen to be sensitive to the amount of water and coke in the process. When the moisture and coke powder content are varied by only a small amount, the technical indexes of the sintering process are seen to fluctuate greatly. Consequently, the sintering process of the high-alumina limonite powders H and J requires a high content of coke powder and moisture, and a low sintering yield, tumble strength index, and productivity index are obtained. Therefore, it is necessary to add a certain amount of magnetite powder into the sintering mixture and then improve the quality of the sinters by optimizing the ore blending and adjusting the basicity.

Sintering of Blends Containing High Proportions of High-Alumina Limonite. The sintering tests were performed at a fixed basicity of 1.9 and an MgO content of 2.3% using the following three blends: **Blend 3** consisting of a 45:10:15:25:5 ratio of powder H, powder J, powder K, fine D, and fine T; **Blend 4** with a 45:15:35:5 ratio of powder H, powder J, fine D, and fine T; and **Blend 5** with a 50:15:25:10 ratio of powder H, powder J, fine D, and fine T. The effects of varying the moisture content and coke dosage for each of the three ore blending schemes are indicated in Table 8.

Here, it can be seen that substituting the low-alumina powder K for a proportion of powders H and J does not produce the ideal sinter. Hence, powder K is excluded from **Blends 4** and **5**, and the dosage of magnetite is increased accordingly. The magnetite crystal is an equiaxed crystal system, whereas the hematite is a hexagonal system. Hence, changes in the lattice structure occur during the sintering process, and these enhance the migration ability of atoms within the structure, which is conducive to the formation of bonds between adjacent particles, thereby improving the strength of the sinter.[34] The present results also indicate that the introduction of an appropriate amount of magnetite concentrates into the high-alumina limonite ore can significantly improve the granulation effect of the mixture and the quality of the sinter, while, concomitantly, significantly reducing the amount of coke powder. After optimizing the ore distribution, the ratio of powders H and J is 65.0% in **Blend 5**, and the optimum sintering index is obtained under the optimum moisture and coke dosage conditions. Therefore, **Blend 5** is selected for further experiments.

Sintering Optimization of Blends with High Proportions of High-Alumina Limonite. For ores with 2.3% MgO, the effects of varying the basicity, moisture content, and coke dosage upon the sintering quality indexes of the blends are presented in Table 9.

Here, the sinter exhibits the highest quality index when the basicity reaches 1.8, giving a sinter yield, tumbling index, and productivity of 75.26%, 61.53%, and 1.2 t·m^{-2}·h^{-1}, respectively. When the basicity reaches 2.0, the quality is seen to diminish, and the lowest quality is observed at a basicity of 1.9. This may be attributed to the initial decrease and subsequent increase in the tumbling strength of the sinter with the increase in basicity.

MICROSTRUCTURE OF THE SINTER

Main Mineral Composition of the Sinter. In this section, the optimal sinter samples of **Blend 5** with three basicity levels are selected for the ore facies identification. The detailed

https://doi.org/10.1021/acsomega.2c07659
ACS Omega 2023, 8, 15951−15959

component composition by percentage is shown in Table 10. Thus, the sinter is seen to be mainly composed of magnetite (Fe_3O_4), hematite (Fe_2O_3), four-dimensional calcium ferrite (SFCA), SS (silicate containing Ca, Fe, Al, Ti, Mg, and other elements), fayalite ($2FeO{\cdot}SiO_2$, $CaO{\cdot}FeO{\cdot}SiO_2$), magnesium ferrite ($MgO{\cdot}Fe_2O_3$), calcium silicate ($2CaO{\cdot}SiO_2$, $CaO{\cdot}SiO_2$), and vitreous and free CaO.

As shown in Figure 3, the main binding phase ratio of the high-alumina limonite sinter is relatively low, which is the main

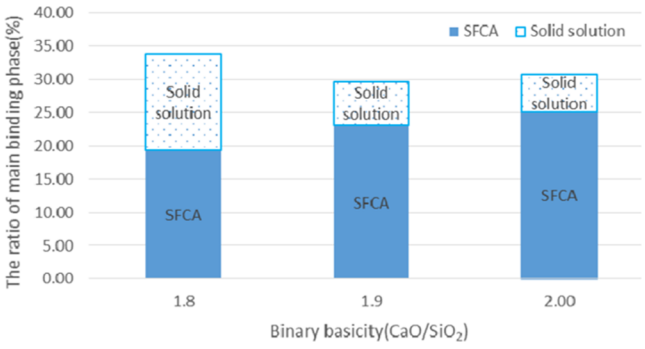

Figure 3. Comparison of the ratio of main binding phase at different basicity.

reason for the decline in the strength and other indexes. Concurrently, with increasing basicity, the content of SFCA in the sinter is seen to gradually increase, while the other main binding phase (a mutual solution of silicate containing Ca, Fe, Al, Mg, and other elements) decreases drastically.

Microstructural Characteristics of the Sinter. The ESEM images of the SFCA in the sinter under various basicity conditions are presented in Figure 4, where the SFCA exhibits a dark gray color due to the high content of aluminum in the mixture. Further, the scanning results in Table 11 indicate that an increase in the Al_2O_3 content of the mixture results in an

Table 11. SEM Results of SFCA at Different Basicities /%

basicity		Fe	Ca	Al	Si	O
1.8	Wt	54.1	8.9	6.0	3.3	27.7
	At	29.6	6.8	6.8	3.6	53.2
1.9	Wt	49.3	10.2	7.9	4.5	28.1
	At	26.3	7.6	8.8	4.7	52.6
2.0	Wt	47.8	11.0	9.0	5.1	27.1
	At	25.6	8.2	10.0	5.4	50.8

increased Al_2O_3 activity as well as a stronger thermodynamic binding tendency of Al_2O_3 with CaO rather than Fe_2O_3. Thus, the incorporation of a simple calcium ferrite or dicalcium ferrite to form the four-dimensional SFCA is a simple strategy for promoting the chemical potential. Meanwhile, the ferrite liquid phase plays a crucial role in cementation and also provides the sinter with the highest strength and the most effective reduction of minerals. As the basicity is increased, the formation of SFCA is gradually increased. Thus, at a basicity of 1.8, the formation of SFCA in the sinter is relatively low, and the crystals are small (Figure 4). At a basicity of 1.9, the amount of SFCA has increased, and the crystals have become thick, stripe-shaped, and columnar. Moreover, when the basicity is increased to 2.0, the SFCA content reaches a maximum (25.1%), and the crystalline grains are thicker. The results in Figure 4 also indicate that some of the solid iron oxide phases are surrounded by the SFCA, thereby increasing the binding force of the liquid−solid phase. This, in turn, increases the strength of the sinter.

As SFCA is one of the main minerals in the binding phase of the aluminum-containing sinter, a greater SFCA content produces a stronger sinter. This suggests that the mixture with a basicity of 2.0 should exhibit the highest sintering index.

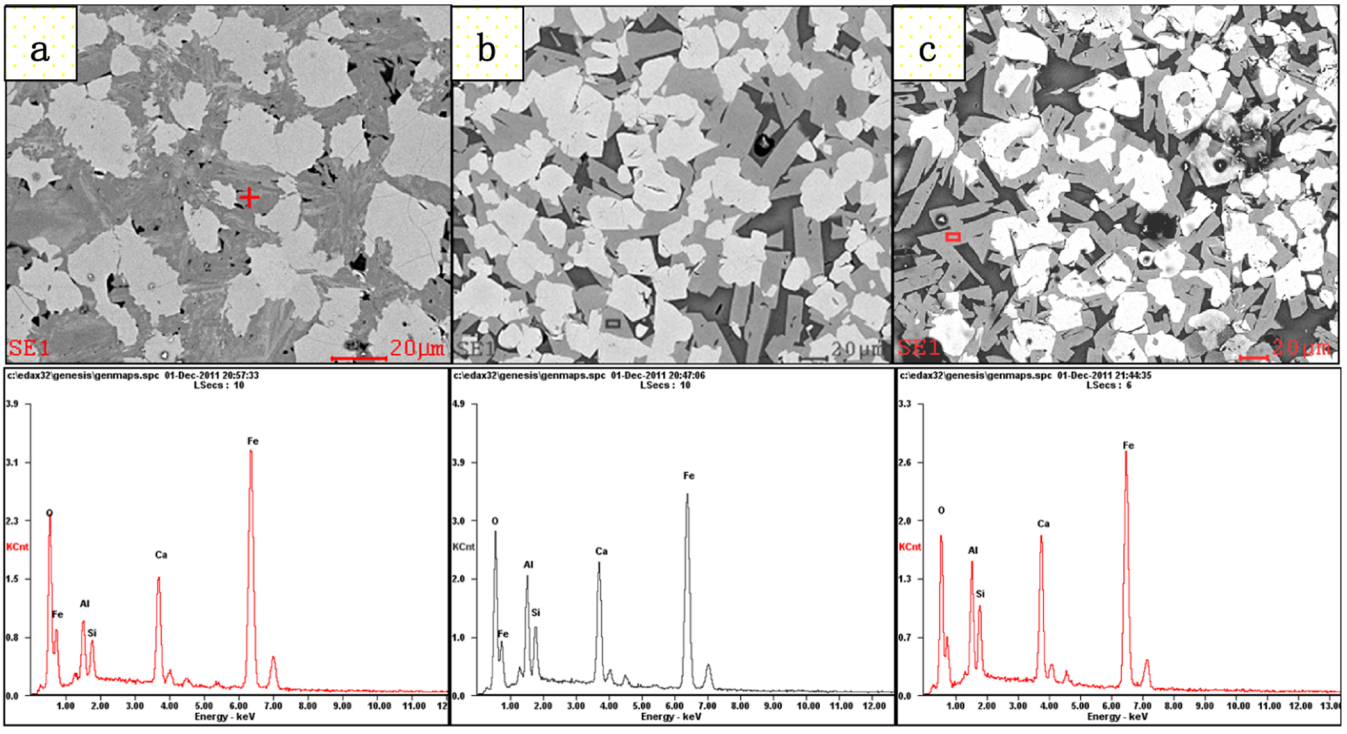

Figure 4. SEM energy spectrum of SFCA at different basicities (a) 1.8, (b) 1.9, and (c) 2.0.

https://doi.org/10.1021/acsomega.2c07659
ACS Omega 2023, 8, 15951−15959

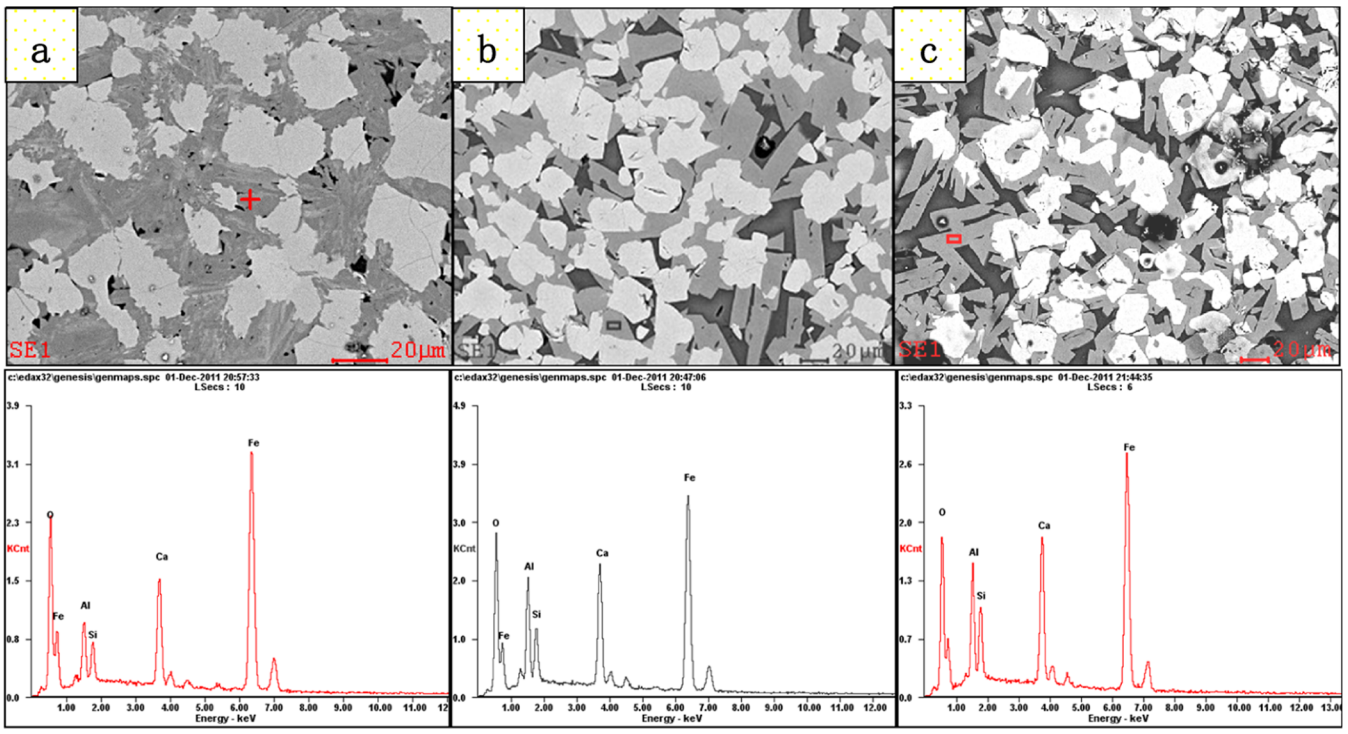

Figure 5. SEM energy spectrum of mutual solution at different basicities: (a) 1.8, (b) 1.9, and (c) 2.0.

However, due to the high proportion of high-alumina limonite in the present study, the sinter index is also affected by other factors. Another major binding phase of the sinter, but obtained under different basicity, is the mutual solution. This consists of silicate containing Ca, Fe, Al, Ti, Mg, and other elements. The ESEM images of the mutual solution phase are presented in Figure 5, and the scanning results are presented in Table 12.

Table 12. SEM Results of Mutual Solution at Different Basicities/%

basicity		Fe	Ca	Al	Si	Ti	O
1.8	Wt	9.0	24.0	5.3	19.8	6.7	35.2
	At	4.0	15.0	4.8	17.7	3.5	55.0
1.9	Wt	30.0	24.2	0.0	10.3	7.6	27.9
	At	15.7	17.7	0.0	10.7	4.7	51.2
2.0	Wt	11.3	33.4	0.0	17.0	7.6	30.7
	At	5.4	22.4	0.0	16.2	4.3	51.7

The results in Figure 5, along with those in Figure 3 and Table 10, indicate that the content of the mutual solution in the sinter is significantly decreased with the increase in basicity. When the content of calcium ferrite in the sinter is low, this silicate liquid phase plays a crucial role in increasing the strength of the sinter.[35] Moreover, when the basicity is 1.8, the content of mutual solution is equivalent to that of SFCA in the sinter (Table 12); this slightly lower-strength liquid phase occupies 14.49% of the sintered mineral phase and is closely bonded with the Fe_2O_3 and Fe_3O_4 particles, thereby supporting the strength of the sinter together with the SFCA. When the basicity is increased to 1.9 or 2.0, however, the amount of mutual solution is decreased sharply, while the SFCA content increases slightly. At the same time, more limestone particles are incorporated, and these require substantial heat for decomposition. As a result, under the optimal condition of 5.8% coke, increasing the basicity is equivalent to decreasing the sintering temperature. Furthermore, the free CaO content in the sinter is seen to increase with the increase in basicity (Table 12). This is further evidenced by the appearance of white spots due to the presence of free CaO in the cross-sectional SEM image of the sinter at a basicity of 2.0. This component easily absorbs water, thereby decreasing the sinter strength. Moreover, the addition of more limestone leads to an increase in the amount of Fe_2O_3 crystals in the sinter. Thus, when the basicity is 2.0, many unbound crystals are observed, and the liquid phase is cemented to the sinter, thereby resulting in low structural strength.

In brief, the SFCA and the mutual solution phases are the main binding phases of the high-alumina limonite sinter, and both phases provide strength to the sinter when a suitable basicity is used. In addition, the microstructure and phase analyses demonstrate that it is possible to increase the amount of SFCA by increasing the basicity, although this sharply lowers the

Table 13. Metallurgical Properties of the Sinter

	low-temperature reduction degradation index (RDI)/%							
basicity	$RDI_{+6.3\ mm}$	$RDI_{+3.15\ mm}$	$RDI_{-0.5\ mm}$	reducibility index (RI)/%	T_{SS} /°C	T_{ES} /°C	$\triangle T_S$ /°C	T_D /°C
1.8	79.3	89.6	3.9	75.6	1141	1209	68	1407
1.9	70.4	85.0	5.1	81.9	1073	1200	127	1379
2.0	53.1	75.1	8.3	81.3	1040	1152	112	1372

https://doi.org/10.1021/acsomega.2c07659
ACS Omega 2023, 8, 15951−15959

amount of mutual solution.[36] Furthermore, increases in the amount of free CaO and granular Fe_2O_3 crystals in the sinter affect the structure and decrease the strength of the sinter.

METALLURGICAL PROPERTIES OF THE SINTER

The effects of basicity on the reducibility, low-temperature reduction degradation, and high-temperature soft melting properties of the sinters are indicated in Table 13.

$RDI_{+6.3\ mm}$, $RDI_{+3.15\ mm}$, $RDI_{-0.5\ mm}$: after being rotated by the drum for 10 min, the mass proportion of particle size fractions of +6.3 mm, 3.15−6.3 mm, and −0.5 mm, respectively, in the sample; RI: reducibility index; T_{SS}: temperature point at 10% of total height shrinkage of the sinter; T_{ES}: temperature point at 40% of total height shrinkage of the sinter; T_D: temperature point at which the liquid phase of the sintered ore sample begins to drip; $\triangle T_S$: softening range.

Here, the three types of sinter each exhibit a high reduction degradation index (RDI) that decreases with the increase in basicity. Meanwhile, the reducibility is seen to increase with the basicity. With respect to the high-temperature soft melting properties, the sinter with a basicity of 1.8 exhibits a narrower soft melting interval and higher dripping temperature than those observed at other basicities. This results in an increased permeability and is beneficial to BF production. Therefore, the sinter with a basicity of 1.8 exhibits the highest index regardless of its RDI or high-temperature soft melting properties. Hence, the metallurgical properties of this sinter can meet the requirements for smelting in small and medium BFs.

CONCLUSIONS

(1) The sintering of high-alumina limonite in the absence of magnetite powder requires a high coke dosage, and the optimum range of coke dosage is narrow. By optimizing the ore blend and adjusting the basicity, the ratio of coke dosage is effectively reduced, and the sintering quality index is improved.

(2) The microstructure of the sinter indicates that, due to the high content of Al_2O_3, the main liquid phase is the silico-ferrite of calcium and aluminum (SFCA), followed by a mutual solution. The SFCA and the mutual solution provide synergistic support to the strength of the sinter. However, the basicity has a great influence on the formation of SFCA and the mutual solution. Thus, when the basicity is increased from 1.8 to 2.0, the amount of SFCA is gradually increased, whereas the amount of mutual solution is drastically decreased.

(3) Under the optimal ore blending conditions, the sinter with a basicity of 1.8 has good microstructural and metallurgical properties, thereby meeting the requirements of medium and small BF smelting conditions, enabling the use of high-alumina limonite with a proportion of 60.0−65.0%, and greatly reducing the sintering production cost.

AUTHOR INFORMATION

Corresponding Authors

Jun Chen − *Hunan Provincial Key Laboratory of Xiangnan Rare-Precious Metals Compounds and Applications, School of Chemistry and Environmental Science, Xiangnan University, Chenzhou 423000, China;* orcid.org/0000-0001-8571-2194; Phone: (+86) 0735 2653128; Email: chenjun4174@126.com

Zhucheng Huang − *School of Minerals Processing & Bioengineering, Central South University, Changsha, Hunan 410083, China*; Phone: (+86) 0731 88830542; Email: zchuangcsu@126.com

Authors

Zhikai Liang − *Hunan Provincial Key Laboratory of Xiangnan Rare-Precious Metals Compounds and Applications, School of Chemistry and Environmental Science, Xiangnan University, Chenzhou 423000, China;* orcid.org/0000-0002-2488-6921

Boyang Huang − *Singapore Centre for 3D Printing, School of Mechanical Aerospace and Engineering, Nanyang Technological University, Singapore 639798, Singapore*

Complete contact information is available at: https://pubs.acs.org/10.1021/acsomega.2c07659

Notes

The authors declare no competing financial interest.

ACKNOWLEDGMENTS

The authors would like to express thanks to the Natural Science Foundation of China (Grant No. 51504230), the Basic Research on the Application of the Cultivation Plan of Scientific and Ttechnological Innovation Ability of Chenzhou Bureau of Science and Technology (Grant No. 2021JCYJ02), the Scientific Research Project of Hunan Provincial Department of Education (Grant No. 20C1724), and the Innovation Training Program for College Students in Hunan Province (Grant No. 202210545005) for financial support of this research.

REFERENCES

(1) Ferreira, H.; Leite, M. G. P. A life cycle assessment study of iron ore mining. *J. Cleaner Prod.* **2015**, *108*, 1081−1091.

(2) Li, Q. F.; Dai, T.; Wang, G. S.; Cheng, J. H.; Zhong, W. Q.; Wen, B. J.; Liang, L. Iron material flow analysis for production, consumption, and trade in China from 2010 to 2015. *J. Cleaner Prod.* **2018**, *172*, 1807−1813.

(3) Wang, Y. Z.; Liu, Z. J.; Zhang, J. L.; Mao, R.; Zhang, Y. P. Advanced converter sludge utilization technologies for the recovery of valuable elements: A review. *J. Hazard. Mater.* **2020**, *381*, No. 120902.

(4) Wu, F. F.; Cao, Z. F.; Wang, S.; Zhong, H. Novel and green metallurgical technique of comprehensive utilization of refractory limonite ores. *J. Cleaner Prod.* **2018**, *171*, 831−843.

(5) Harvey, L. D. Iron and steel recycling: Review, conceptual model, irreducible mining requirements, and energy implications. *Renewable Sustainable Energy Rev.* **2021**, *138*, No. 110553.

(6) Wu, S.; Han, H.; Ma, L.; Jiang, W.; Liu, X.; Zhang, L. Optimization of Flux Composition for Sintering With High Limonite Proportion. *J. Iron Steel Res. Int.* **2009**, *16*, 200−204.

(7) Abd Rashid, R. Z.; Salleh, H. M.; Ani, M. H.; Yunus, N. A.; Akiyama, T.; Purwanto, H. Reduction of low-grade iron ore pellet using palm kernel shell. *Renewable Energy* **2014**, *63*, 617−623.

(8) Wu, F. F.; Cao, Z. F.; Wang, S.; Zhong, H. Phase transformation of iron in limonite ore by microwave roasting with addition of alkali lignin and its effects on magnetic separation. *J. Alloys Compd.* **2017**, *722*, 651−661.

(9) Fu, J. Y.; Jiang, T.; Zhu, D. Q. *Sintering and Pelleting*, 2nd ed.; Fan, M., Ed.; Academic Press: Changsha, 1996; pp 36−39.

(10) Palmero, P.; Lombardi, M. Sintering of a nano-crystalline metastable alumina: influence of the firing parameters on the phase development and microstructural evolution. *J. Therm. Anal. Calorim.* **2009**, *97*, 191−196.

(11) Djangang, C. N.; Tchamba, A. B.; Kamseu, E.; Melo, U. C.; Elimbi, A.; Ferrari, A. M.; Leonelli, C. Reaction sintering and

microstructural evolution in metakaolin-metastable alumina composites. *J. Therm. Anal. Calorim.* **2014**, *117*, 1035−1045.
(12) Hu, L. *Influence and Mechanism of Al_2O_3 and SiO_2 on Iron Ore Sintering*; Thesis database of Central South University: Changsha, 2011; pp 23−29.
(13) Mazanek, E.; Jasienska, S. Formation of binary ferrites in iron ore sinters. *Iron Steel Inst. J.* **1996**, *204*, 344−348.
(14) Choudhary, M. K.; Nandy, B. Effect of flame front speed on sinter structure of high alumina iron ores. *ISIJ Int.* **2006**, *46*, 611−613.
(15) Guo, H.; Guo, X. M. Effect of alumina on liquid phase formation in sintering process of iron ore fines. *Steel. Res. Int.* **2019**, *90*, No. 1900138.
(16) Lu, L.; Holmes, R. J.; Manuel, J. R. Effects of alumina on sintering performance of hematite iron ores. *ISIJ Int.* **2007**, *47*, 349−358.
(17) Sinha, M.; Ramna, R. V. Effect of variation of alumina on the microhardness of iron ore sinter phases. *ISIJ Int.* **2009**, *49*, 719−721.
(18) Umadevi, T.; Sah, R.; Mahapatra, P. C. Influence of sinter basicity (CaO/SiO_2) on low and high alumina iron ore sinter quality. *Miner. Process. Extr. Metall.* **2013**, *123*, 75−85.
(19) Scarlett, N. V. Y.; Pownceby, M. I.; Madsen, I. C.; Christensen, A. N. Reaction sequences in the formation of silico-ferrites of calcium and aluminum in iron ore sinter. *Metall. Mater. Trans. B* **2004**, *35*, 929−936.
(20) Fukuda, K.; Takeda, A.; Yoshida, H. Remelting reaction of α-Ca_2SiO_4 solid solution confirmed in Ca_2SiO_4−$Ca_{12}Al_{14}O_{33}$ pseudobinary system. *Cem. Concr. Res.* **2001**, *31*, 1185−1189.
(21) Oluwadare, G. O. Roles of alumina and magnesia on the formation of SFCA in iron ore sinters. *Trends Appl. Sci. Res.* **2007**, *2*, 483−491.
(22) Webster, N. A. S.; Pownceby, M. I.; Madsen, I. C.; Kimpton, J. A. Silico-ferrite of calcium and aluminum (SFCA) iron ore sinter bonding phases: new insights into their formation during heating and cooling. *Metall. Mater. Trans. B* **2012**, *43*, 1344−1357.
(23) Hessien, M. M.; Kashiwaya, Y.; Ishii, K.; Nasr, M. I.; El-Geassy, A. A. Sintering and heating reduction processes of alumina containing iron ore samples. *Ironmaking Steelmaking* **2008**, *35*, 191−204.
(24) Wu, S.; Zhang, G. Liquid absorbability of iron ores and large limonite particle divided adding technology in the sintering process. *Steel Res. Int.* **2015**, *86*, 1014−1021.
(25) Zhu, Z. P.; Jiang, T.; Li, G. H.; Huang, Z. C. Thermodynamics of reaction of alumina during sintering process of high-iron gibbsite-type bauxite. *Chin. J. of Nonferrous Met.* **2009**, *19*, 2243−2250.
(26) Choudhary, M. K.; Bhattacharjee, D.; Bannerjee, P. S.; Lahiri, A. K. Effect of variation of alumina on development of phases during iron ore sintering. *ISIJ Int.* **2008**, *48*, 1804−1806.
(27) Umadevi, T.; Prakash, S.; Bandopadhyay, U. K.; Mahapatra, P. C.; Prabhu, M.; Ranjan, M. Influence of alumina on iron ore sinter quality and productivity. *World Iron Steel* **2010**, *10*, 12−18.
(28) Shen, T.; Chen, W. Experimental study and application about large proportion brown iron ore sintering. *Min. Metall.* **2010**, *19*, 75−78.
(29) Kalenag, K. M.; Garbers-craig, M. A. Investigation into how the magnesia, silica, and alumina contents of iron ore sinter influences its mineralogy and properties. *J. South. Afr. Inst. Min. Metall.* **2010**, *110*, 447−456.
(30) Dong, J. J.; Wang, G.; Gong, Y. G.; Xue, Q. G.; Wang, J. S. Effect of high alumina iron ore of gibbsite type on sintering performance. *Ironmaking Steelmaking* **2015**, *42*, 34−40.
(31) Liu, D. H.; Liu, H.; Zhang, J. L.; Liu, Z. J.; Xue, X.; Wang, G. W.; Kang, Q. F. Basic characteristics of Australian iron ore concentrate and its effects on sinter properties during the high-limonite sintering process. *Int. J. Miner., Metall. Mater.* **2017**, *24*, 991−998.
(32) Wu, S. L.; Zhai, X. B.; Su, L. X.; Ma, X. D. Ore-blending optimization for Canadian iron concentrate during iron ore sintering based on high-temperature characteristics of fines and nuclei. *J. Iron Steel Res. Int.* **2020**, *27*, 755−769.
(33) Huang, Z. C.; Liang, Z. K.; Yi, L. Y.; Jiang, T. Metallogenic mechanism of sintering of high ratio of high alumina limonite. *J. Cent. South Univ.* **2014**, *45*, 1013−1020. (In Chinese)
(34) Zhu, D. Q.; Xue, Y. X.; Pan, J.; Yang, C. C.; Guo, Z. Q.; Tian, H. Y.; Liao, H.; Pan, L. T.; Huang, X. Z. An investigation into the distinctive sintering performance and consolidation mechanism of limonitic laterite ore. *Powder Technol.* **2020**, *367*, 616−631.
(35) Liu, D. M.; Loo, C. E.; Evans, G. Flow characteristics of the molten mix generated during iron ore sintering. *Int. J. Miner. Process.* **2016**, *149*, 56−68.
(36) Sinha, M.; Nistala, S. H.; Chandra, S.; Mankhand, T. R. Mineralogy of iron ores of different alumina levels from Singhbhum belt and their implication on sintering process. *J. Miner. Mater. Charact. Eng.* **2015**, *03*, 180−193.

https://doi.org/10.1021/acsomega.2c07659
ACS Omega 2023, 8, 15951−15959